Research Article | Vol. 33, No. 24 / 1 Dec 2025 / Optics Express 51351
Optics EXPRESS

# Statistical characterization of discrete amplitude-modulated coherent states at telecom wavelengths by means of an up-conversion-based photon-number-resolving detector

SILVIA CASSINA, ALEX POZZOLI, AND ALESSIA ALLEVI*

*Como Lake Institute of Photonics, Department of Science and High Technology, University of Insubria, Via Valleggio 11, I-22100 Como, Italy*
*alessia.allevi@uninsubria.it

**Abstract:** The successful implementation of quantum communication protocols relies on the proper encoding of information in the degrees of freedom of the employed optical states. Particular interest is devoted to amplitude-phase-shift keying coherent states, which can provide robust solutions in satellite communication systems and guarantee high values of channel capacity. In this work, we implement a sum-frequency-based photon-number-resolving detector, capable of revealing discrete amplitude modulation of coherent states produced at telecom wavelengths. The detection is performed in the visible spectral range and in the photon-number-resolving domain, thus encouraging the use of more complex alphabets in which both amplitude and phase vary.



## 1. Introduction

The realization of communication protocols, such as those devoted to quantum key distribution (QKD), is based on the use of a proper encoding alphabet and an efficient receiver able to decrypt a key or decode a message [1–5]. In the case where the encoding is performed with coherent states [6–8], information can be carried out by their intensity and phase. These quantities can be modulated either in a continuous (or at least approximately continuous) [9–11] or in a discrete way [12–15], depending on the specific protocol and on the adopted receiver. For instance, one of the commonly used encodings is represented by phase-shift keying (PSK), which employs an alphabet with $N$ coherent states $|\alpha_k\rangle = |ae^{i(2\pi/N)k}\rangle$ with relative phases $(2\pi/N)k$ and fixed amplitude $a$ [16–20]. More complex variations are given by PSK signals with different amplitude levels, usually called amplitude-phase-shift keying (APSK), which have long been recognized to be a robust constellation of states to deal with nonlinear amplifier distortions in satellite communication systems [21–25]. Moreover, in the framework of continuous variable (CV) QKD, a suitable probabilistic amplitude shaping of a finite set of symbols allows to approximate at will the optimal channel capacity [26]. The typical receiver employed to detect such states is represented by optical homodyne detection [3,27,28]. However, also direct detection schemes with partial photon-number-resolving (PNR) capabilities can be employed to this aim [29]. Among them, we have recently realized a homodyne-like detection scheme based on Silicon photomultipliers (SiPMs) that can be of use to discriminate binary PSK coherent states [30] as well as to implement CV-QKD protocols [31].

The main limitation of the current PNR detectors is given by their sensitivity, which is mainly confined in the visible spectral range, while quantum communication protocols exploit the infrastructure of optical fibers working in the C-band of wavelengths [32–35]. That is why we have recently developed a sum-frequency-based PNR detector that exploits the up-conversion process to convert telecom wavelengths into visible ones, and SiPMs to guarantee PNR capability.

#576205 https://doi.org/10.1364/OE.576205
Journal © 2025 Received 12 Aug 2025; revised 1 Oct 2025; accepted 29 Oct 2025; published 25 Nov 2025

Optics EXPRESS

The same idea has been already explored with the old generation of SiPMs, affected by a non-negligible optical cross talk, to convert light from the near infrared to the visible spectral range [36,37], and, more recently, with a different model of SiPMs from mid-infrared wavelengths to near-infrared ones [38]. Our recent work [39] has been devoted to prove the capability of our detection system of studying the stability condition of a telecom light source produced by white light continuum (WLC) followed by an optical parametric amplifier (OPA), showing that the Poissonian character of the source is attained only by exceeding the critical power for self-focusing by a few times [40]. Fixed the suitable condition, in this proof-of-principle work we focus on the possibility to modulate the telecom light source and reveal the effect of such a modulation by measuring the up-converted beam. In particular, we operate a discrete amplitude modulation and reconstruct the statistical properties of the modulated light in terms of detected photons. This characterization represents a crucial and fundamental step towards the realization of a detection scheme more suitable for quantum communication applications. In fact, in this work we simply consider a direct detection scheme, in which we can have access both to the photon-number distributions of the single outputs and to the photon-number correlations between the two outputs. Viceversa, the application of the receiver to quantum communication protocols requires the implementation of a homodyne-like interferometric scheme [31] operating at telecom wavelengths. This also implies the production of a low-intensity local oscillator (LO) that should be converted as well from telecom wavelengths to the same wavelength as the signal states. In view of the future exploitation of the receiver, the results achieved so far seem really promising and suggest the implementation of more complex modulations of both amplitude and phase in order to take full advantage of the versatility of the detector.

## 2. Theoretical description

The implemented detection system is based on the realization of a sum-frequency process according to a collinear interaction geometry and under parametric approximation. This means that one of the two beams interacting in the nonlinear crystal is considered as an undepleted pump beam, while the other beam is evolving as well as the generated one [41]. Under this assumption, the intensity of the generated beam is directly proportional to the one of the other evolving beam interacting in the nonlinear medium. A more complex dependence should be considered if the phase-matching condition is not completely satisfied. In that case the sum-frequency generation process produces a less efficient up-converted beam, in which the intensity of the generated beam is modulated by a $\mathrm{sinc}^2(x)$ function [41].

The proportionality between up-converted and input beams is also responsible for the conservation of the statistical properties, especially in terms of photon-number distributions. This means that if the input beam is described by a Poissonian distribution, the same holds for the up-converted one [42,43]. More interestingly, a proper amplitude modulation of the input beam leads to an amplitude-modulated up-converted beam. Having at our disposal a detection system based on PNR detectors, these features can be deeply investigated by considering the reconstruction of photon-number distributions, as well as studying their moments and photon-number correlations obtained by dividing the up-converted light at a balanced beam splitter (BS) [44]. These characterizations represent a first and necessary step to prove the reliability of the detection system in view of its applications in the quantum communication context, even though to this aim the experimental scheme will be more complex. In fact, it will involve a Mach-Zehnder intereferometer, in which the signal state will be mixed with a low-intensity LO that will be converted as well as the signal from telecom wavelengths to visible ones. In particular, in this work we are interested in studying the statistical properties that emerge from a discrete modulation of the input beam, that is combining together two or more Poissonian distributions according to a scaling configuration [45,46]. In particular, if we consider the Poissonian distribution for

Optics EXPRESS

detected photons

$$P(m) = \frac{\langle m \rangle^m}{m!} \exp\left(-\langle m \rangle\right), \tag{1}$$

a linear combination of this kind of distribution with different weights reads as

$$P_{\mathrm{mod}}(m) = \sum_{i=1}^{N} p_i \frac{\langle m_i \rangle^m}{m!} \exp\left(-\langle m_i \rangle\right), \tag{2}$$

where $p_i$ is the weight of the i-th Poissonian distribution with mean value $\langle m_i \rangle$, $N$ is the total number of discrete modulation steps adopted, and $\sum_{i=1}^{N} p_i = 1$. The presence of an amplitude modulation introduces photon-number correlations by dividing the light at a BS. This behavior can be investigated by calculating the first two moments of the distributions in Eq. (2), which can be expressed as

$$\langle m_{\mathrm{mod}} \rangle = \sum_{m=0}^{\infty} m\, P_{\mathrm{mod}}(m) \tag{3}$$

$$\langle m_{\mathrm{mod}}^2 \rangle = \sum_{m=0}^{\infty} m^2\, P_{\mathrm{mod}}(m). \tag{4}$$

From their combination, it is possible to calculate the variance of the distribution $\sigma^2_{\mathrm{mod}}(m) = \langle m^2_{\mathrm{mod}} \rangle - \langle m_{\mathrm{mod}} \rangle^2$ and hence the Fano factor, which is defined as $F_{\mathrm{mod}}(m) = \sigma^2_{\mathrm{mod}}(m)/\langle m_{\mathrm{mod}} \rangle$. Indeed, it is possible to demonstrate that the photon-number correlation coefficient, defined as

$$\Gamma(m_1, m_2) = \frac{\langle (m_1 - \langle m_1 \rangle)(m_2 - \langle m_2 \rangle) \rangle}{\sqrt{\sigma^2(m_1)\, \sigma^2(m_2)}}, \tag{5}$$

in which $m_1$ and $m_2$ are the number of photons detected at the two BS outputs, can be expressed in terms of the Fano factor of the light impinging on the BS [47]. In the case of a balanced BS and the amplitude modulated light statistically described by Eq. (2),

$$\Gamma(m_1, m_2) = \frac{F_{\mathrm{mod}} - 1}{F_{\mathrm{mod}} + 1}, \tag{6}$$

in which $F_{\mathrm{mod}}$ is the Fano factor corresponding to the light impinging on the BS. The calculation of the correlation coefficient allows us to better investigate the statistical properties of the modulated light since it is based on the first two moments of the investigated distributions. In particular, as shown hereafter it is sensitive to the number of modulation steps we consider and also to their weights.

## 3. Experimental setup

The setup we realized to investigate the possibility to detect an amplitude modulated light beam at telecom wavelengths thanks to the sum-frequency-based PNR detector is shown in Fig. 1(a). Since we do not have at our disposal a pulsed light source at telecom wavelengths, light pulses at 1550 nm are obtained by sending the sub-picosecond pulses ($\sim$ 190 fs) at 1038 nm of an amplified Yb:KGW laser operated at 3 kHz to a yttrium aluminium garnet (YAG) plate to produce WLC both in the visible spectral range and in the near infrared (up to 1600 nm). Then the pulses at 1550 nm are amplified thanks to an OPA pumped by the second harmonic of the laser. An amplification gain of $\sim 10^4$ is obtained by means of a slightly noncollinear interaction geometry between the pump beam and the infrared one in a $\beta$-Barium-Borate crystal (BBO, cut angle = 23.4°, 3 mm long) [39]. A typical spectrum of the amplified light beam at 1550 nm, obtained

Optics EXPRESS

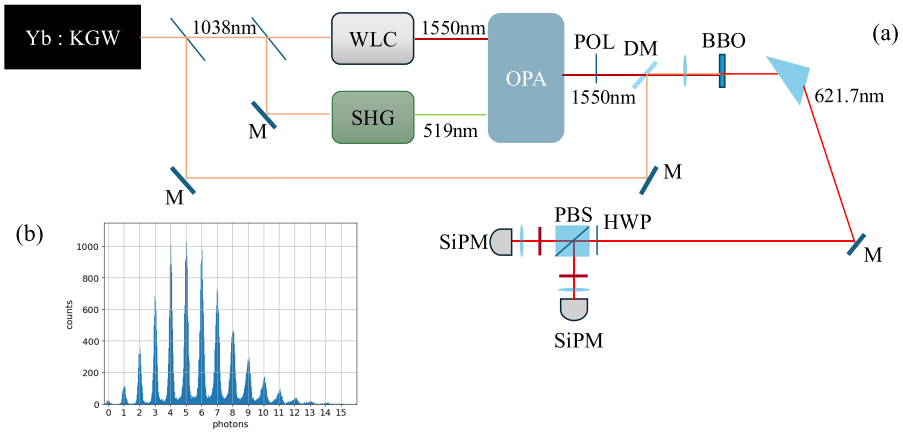


**Fig. 1.** (a) Schematic of the experimental setup. WLC: white light continuum, SHG: second-harmonic generation; OPA: optical parametric amplifier; POL: polarizer; DM: dichroic mirror; BBO: $\beta$-Barium-Borate crystal; M: mirror; HWP: half-waveplate; PBS: polarizing cube beam splitter; SiPM: Silicon photomultiplier. (b) Typical pulse height spectrum of a SiPM in the case of Poissonian light with mean value $\langle m \rangle = 5.85$.

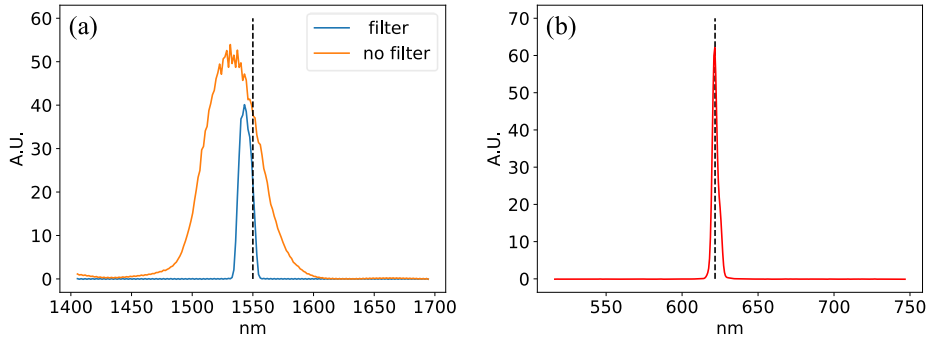


**Fig. 2.** (a) Spectrum of the amplified WLC in the infrared region in the presence (blue curve) and in the absence (orange curve) of a 12 nm wide bandpass filter. The dashed black curve corresponds to 1550 nm. (b) Spectrum of the up-converted light, in which the generation of the sum frequency at 621.7 nm is highlighted by the black dashed line. The spectrum has been obtained using a 10 nm wide bandpass filter centered at 620 nm in front of the spectrometer.

by means of a fiber spectrometer (mod. MiniSpectrometer TG-NIR: C11482GA, Hamamatsu Photonics) placed beyond the BBO crystal, is shown in panel (a) of Fig. 2.

The light beam at telecom wavelengths is suitably filtered by means of a 12 nm wide bandpass filter centered at 1550 nm and transmitted through a dichroic mirror that is used to reflect a portion of the fundamental beam at 1038 nm in order to make the two beams almost collinear beyond the mirror itself. A convergent lens with a focal length of 50 mm focuses the two beams in a further BBO crystal (cut angle = 23.4°, 3 mm long), where they interact to produce by sum-frequency generation an up-converted beam at 621.7 nm. The second-order nonlinear interaction is obtained in a quasi-collinear interaction geometry by micrometrically adjusting the temporal delay of the beam at fundamental wavelength. A typical spectrum of the up-converted light beam at 621.7 nm, obtained by means of a fiber spectrometer (mod. AvaSpec-ULS2048x64-EVO, Avantes) placed beyond the BBO crystal, is shown in panel (b) of Fig. 2. The light beam at 621.7 nm passes

Optics EXPRESS

through a prism, which is used to spatially separate it from the light beams at 1038 and 1550 nm, and then is separated at a polarizing cube beam splitter (PBS) preceded by a half-waveplate (HWP) to obtain two replicas and thus study photon-number correlations. The choice of using a PBS combined with an HWP instead of a BS allows us to fine-tune the balance between the two output signals. At each PBS output, an achromatic doublet, preceded by a 10 nm wide bandpass filter centered at 620 nm, focuses light into a multimode fiber, which delivers it to the detector. Specifically, we employ two SiPMs (mod. MPPC S13360–1350CS, Hamamatsu Photonics), which are detectors endowed with an outstanding PNR capability working at room temperature, as shown in Fig. 1(b). They are constituted by a matrix of 667 squared cells, with a pixel pitch of 50 $\mu$m, operated in the Geiger-Müller regime with a common output. Ideally, the number of fired cells corresponds to the number of incident photons. Deviations from ideality is due to a non perfect quantum efficiency ($\sim$ 25% at the investigated wavelength) and to other drawbacks, such as optical cross talk and dark counts, which, however, are small in this model of SiPMs compared to previous generations or other models with a larger value of pixel pitch. Both effects have been made negligible during the acquisition stage [48–50]. Indeed, the two detector outputs, after being amplified, are synchronously integrated over a 10 ns gate centered around the output peak. This reduces the contribution of cross talk effect below the 1% and that of dark counts to 0.3% [31]. It is important to notice that the adopted boxcar-gated integrators represent the main limitation in terms of bandwidth (100 MHz) and noise, not allowing the reliable detection of light with mean number of photons lower than 0.5. This means that for smaller energy values a different acquisistion system should be used. This choice may also be desirable in view of practical applications to quantum communication, where faster acquisition systems are typically needed. For instance, a recent advance in high-speed PNR detection technologies is reported in Ref. [51]. As already mentioned in the Introduction, the investigation performed in this work is aimed at showing that the detection apparatus including sum-frequency and SiPMs is able to reveal the amplitude modulation introduced on the beam at telecom wavelengths. This is obtained by placing a polarizer in front of the dichroic mirror (POL in Fig. 1) and rotating it in steps of 10°. For each angle, a sequence of 200,000 shots, specifically 4 repetitions of 50,000 shots each, is measured by the two SiPMs. We notice that the choice of reconstructing amplitude-modulated states represents a good test of the reliability of the receiver because their photon-number distribution is not trivial. Furthermore, it could be useful for the realization of communication protocols, such as the one presented in [52], in which the encoding of a given alphabet of symbols is performed not in single shots but instead in a given data sample each. In this case, the PNR capability of our receiver allows us to discriminate whether the analyzed data set corresponds to a single symbol or a combination of two or more symbols.

## 4. Experimental results and discussion

The mean value of light at 1550 nm is shown as a function of the rotation angle of the polaroid in panel (a) of Fig. 3. Each experimental point (dots + error bars) is obtained with the MiniSpectrometer setting the exposure time to 1 ms and acquiring 1000 consecutive traces. The procedure is repeated three times to properly calculate error bars. The fitting function given by Malus law is also shown in the same panel as a solid curve. In panel (b) of the same figure, we show as dots + error bars the sum of the mean values of the light at 621.7 nm measured by the two SiPMs as a function of the same rotation angle. In this case, the fitting function, shown as a solid curve, is given by a $\mathrm{sinc}^2(x)$ function, thus proving that the deviation from the Malus law is due to the phase mismatch effect. Indeed, the non-perfect extinction ratio of the polaroid (<200:1 at 1550 nm) and the use of an interaction configuration with focused beams make the evolution of the generated beam at 621.7 nm more critical than expected under ideal conditions of perfect phase matching. In this regard, an interaction geometry involving collimated light beams could enable a more successful achievement of phase-matching conditions, thus making it possible to

Optics EXPRESS

realize and properly detect phase encoding in addition to amplitude encoding. Apart from these small discrepancies, the beam at 1550 nm and that at 621.7 nm follow the same trend, starting from a maximum value and decreasing to a minimum one. Despite the fact that the data shown in the two panels of the figure are presented on the same scale, it is important to emphasize that the global efficiency of the detection system is around 10%, a value definitely lower compared to what has been recently achieved in all-fiber systems [53]. This is mainly due to the chosen tight focus configuration and to the quantum efficiency of the employed SiPMs, which is ~ 25% at 621.7 nm. Thus, possible improvements to the efficiency of the receiver could be obtained both changing the interaction geometry and adopting new generations of SiPMs with a higher quantum efficiency in the explored spectral range.

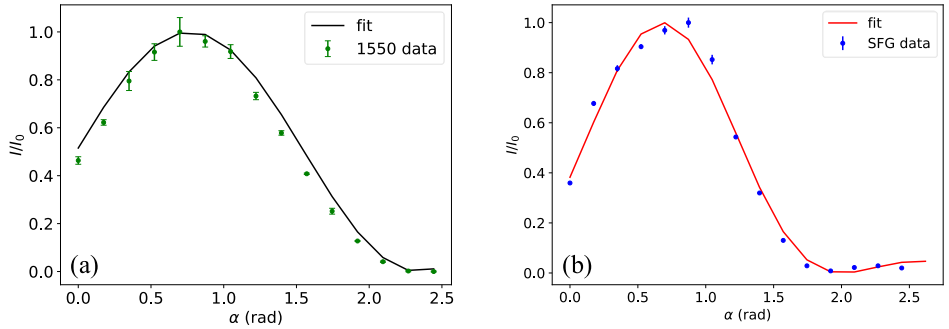


**Fig. 3.** (a) Normalized intensity of light at 1550 nm as a function of the rotation angle of the polaroid. (b) The same as in (a) for light at 621.7 nm (SFG). In both panels the solid curve is the fitting function, which in (a) is proportional to a $\cos^2(x)$ function, while in (b) to a $\mathrm{sinc}^2(x)$ function.

The statistical distribution of red light for each choice of the rotating angle $\alpha$ is Poissonian, as shown in Fig. 4, where the reconstructed experimental distributions for detected photons in the case of $\alpha_1 = 0.7$ rad and $\alpha_2 = 2.1$ rad are shown together with the corresponding theoretical expectations. The Poissonian character of the experimental distributions is quantified considering the fidelity parameter, which is defined as $f = \sum_{m=0}^{\bar{m}} \sqrt{p_{\mathrm{th}}(m) p_{\mathrm{exp}}(m)}$, in which $p_{\mathrm{th}}(m)$ and $p_{\mathrm{exp}}(m)$ are the theoretical and experimental distributions, respectively, and the sum extends up to the maximum number of detected photons, $\bar{m}$, above which both $p_{\mathrm{th}}(m)$ and $p_{\mathrm{exp}}(m)$ become negligible. The high values of $f$ are indicated in the caption of the figure. In addition, the calculation of the correlation coefficient in Eq. (5) returns values below 1.5% for all the considered mean values shown in Fig. 3, thus proving that for each step of modulation the statistical distribution is Poissonian.

Conversely, if two modulation choices are considered together, the measured photon-number distribution changes. As an example, in Fig. 5(a) we show the experimental distributions in the case in which the data corresponding to $\alpha_1 = 0.7$ rad and $\alpha_2 = 2.1$ rad are considered as a unique dataset. As mentioned in Section 2, when a communication protocol in which discrete amplitude modulation is considered, it is useful to investigate the case in which the two modulation amplitudes are chosen with different weights. In particular, the data are shown as a function of $p_1$, which is the weight corresponding to the dataset taken at $\alpha_1$. In the figure the different colors correspond to different weights, assuming that the total number of acquired data is always the same, namely 200,000. As it can be noticed, all the distributions exhibit two peaks: the first one is connected to the original Poissonian distribution with the lowest mean value, and the second one to the original Poissonian distribution with the highest mean value. The different weights determine an increase of either the first or the second peak. All the experimental data are well superimposed on the corresponding theoretical expectations according to Eq. (2). The

Optics EXPRESS

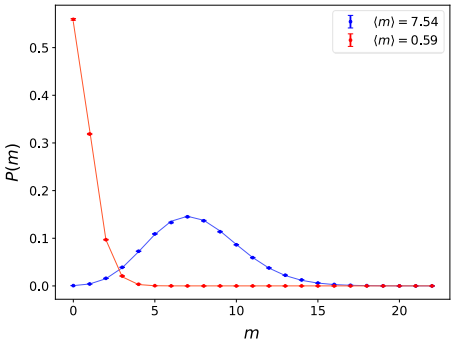


**Fig. 4.** Detected photon-number distributions at two different modulation values, namely at $\alpha_1 = 0.7$ rad (in blue) and $\alpha_2 = 2.1$ rad (in red). Dots + error bars: experimental data; solid curves: theoretical expectations according to Eq. (1). The fidelity values to Poissonian distributions are f = 0.99995 for $\alpha_1$ and f = 0.99991 for $\alpha_2$.

agreement between data and theory can also be investigated in terms of the correlation coefficient: in Fig. 5(b) we show its experimental values as a function of $p_1$. Concerning the behavior, it is worth noting that the absolute values of $\Gamma$ depend on the mean values of the two original distributions, but also on their weights. In fact, explicitly stating these parameters, the correlation coefficient reads as

$$\Gamma = \frac{(\langle m_{\mathrm{H}}\rangle - \langle m_{\mathrm{L}}\rangle)^2 p_1 p_2}{\left[(\langle m_{\mathrm{H}}\rangle - \langle m_{\mathrm{L}}\rangle)^2 p_1 p_2\right] + 2\left(\langle m_{\mathrm{H}}\rangle p_1 + \langle m_{\mathrm{L}}\rangle p_2\right)}, \tag{7}$$

that can be further simplified by taking into account that $p_2 = 1 - p_1$. Note that, in the expression, $\langle m_{\mathrm{H}}\rangle$ and $\langle m_{\mathrm{L}}\rangle$ correspond to the original distributions with the highest and lowest mean value, respectively, before the division at the BS. Instead, it is interesting to notice that the position, *i.e.* the value of $p_1$, corresponding to the maximum value of $\Gamma$ depends only on the ratio $r$ between the mean values of the two original distributions, namely:

$$p_{1,max} = \frac{\sqrt{r}(\sqrt{r} - 1)}{(r - 1)}, \tag{8}$$

where $r = \langle m_{\mathrm{L}}\rangle / \langle m_{\mathrm{H}}\rangle$. Let's consider the case in which the two distributions have mean values $\langle m_{\mathrm{H}}\rangle = 2 \cdot 7.54 = 15.08$ and $\langle m_{\mathrm{L}} =\rangle = 2 \cdot 0.59 = 1.18$ before being divided at the BS. For this choice, we obtain a theoretical behavior of $\Gamma$ as a function of $p_1$ characterized by a decreasing trend with a maximum value at $p_1 \sim 0.21$ (see Fig. 5). Note that when the weight corresponds to having only one of the two original Poissonian distributions, the correlation coefficient drops to 0. The theoretical expectations according to Eq. (6) are shown as open circles in the same plot.

The good results obtained considering only two modulation values suggest further studies. That is why in the following we consider the case of more than 2 modulation amplitudes. In particular, we investigate the case of an even number of modulation values, namely 2, 4, 6 and 8. This means that we consider more than two datasets as a unique one. For simplicity, in this case we assume that all the datasets mixed together have the same weights. The experimental statistical distributions are shown in Fig. 6(a) together with their theoretical expectations according to Eq. (2). We can notice that the larger the number of modulation values the flatter the corresponding distribution. Indeed, a continuous modulation would lead to an amplitude-averaged distribution, similar to what could be obtained by averaging the phases of a coherent state [54,55]. This also explains why the correlation coefficient is a decreasing function of the number of modulation values, $n_{\mathrm{mod}}$. The larger the number, the lower the value of $\Gamma$. The experimental data, shown as

Optics EXPRESS

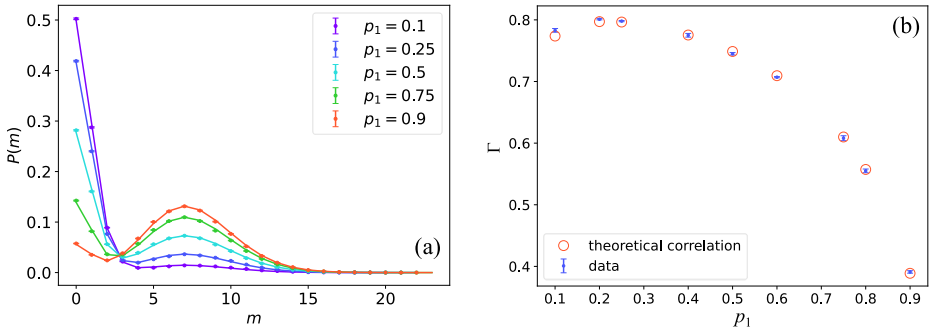


**Fig. 5.** (a) Detected photon-number distributions obtained as a combination of two modulation values with different weights. Dots + error bars: experimental data; solid curves: theoretical expectations according to Eq. (2). The different colors refer to different weight values of the state corresponding to $\alpha_1$: purple to $p_1 = 0.1$, blue to $p_1 = 0.25$, light blue to $p_1 = 0.5$, green to $p_1 = 0.75$, and red to $p_1 = 0.9$. The fidelity values are greater than 0.9999 in all cases. (b) Correlation coefficient $\Gamma$ as a function of the weight $p_1$. Dots + error bars: experimental data; open circles: theoretical expectations according to Eq. (6).

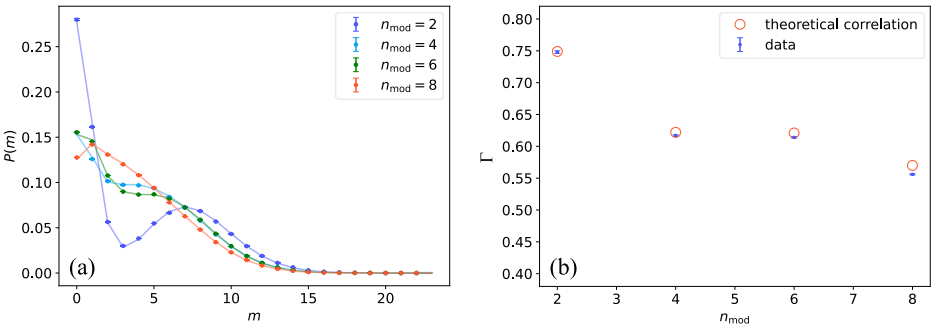


**Fig. 6.** (a) Detected photon-number distributions obtained as a combination of an even number of modulation values with the same weights. Dots + error bars: experimental data; solid curves: theoretical expectations according to Eq. (2). The different colors refer to different number of modulation values, $n_{\mathrm{mod}}$: blue to $n_{\mathrm{mod}} = 2$, light blue to $n_{\mathrm{mod}} = 4$, green to $n_{\mathrm{mod}} = 6$, and red to $n_{\mathrm{mod}} = 8$. The fidelity values are larger than 0.9999 in all cases. (b) Correlation coefficient $\Gamma$ as a function of $n_{\mathrm{mod}}$. Dots + error bars: experimental data; open circles: theoretical expectations according to Eq. (6).

dots + error bars in Fig. 6(b), are almost superimposed on the theoretical expectations, shown as open circles. Possible discrepancies could be ascribed to the non perfect division of light at the BS. However, note that the percent errors are within 2.5%. Concerning the absolute values of $\Gamma$, we notice that the irregular trend as a function of $n_{\mathrm{mod}}$ must be ascribed to the irregular spacing between the mean values of the original states used to build the amplitude-modulated ones. This fact can be investigated by considering what happens if the modulation is built by using a linear variation of the mean value with equal spacing. The theoretical expectation is shown in Fig. 7(a) for different values of $n_{\mathrm{mod}}$, and setting $\langle m_{\mathrm{L}} \rangle = 1$ and $\langle m_{\mathrm{H}} \rangle = 15$. In this case, the decreasing behavior as the values of $n_{\mathrm{mod}}$ increase (up to 1000) is very regular and already reaches an asymptotic value at tens of modulation values. In particular, the behavior corresponding to the first part of the curve ($n_{\mathrm{mod}} \leq 8$) is shown in the inset of panel (a), while in panel (b) of the same figure we show that the absolute values of $\Gamma$ also depend on the energy of the states involved in the modulation. In fact, the larger the energy, the larger the values of the

Optics EXPRESS

correlation coefficient. The achieved results prove that the modulation of the beam at 1550 nm can be properly revealed by our sum-frequency-based PNR detector, thus encouraging the further exploitation of the detection apparatus in more complex encoding alphabets. In particular, it would be interesting to modulate the beam at telecom wavelengths both in amplitude and phase in order to build a constellation of APSK coherent states.

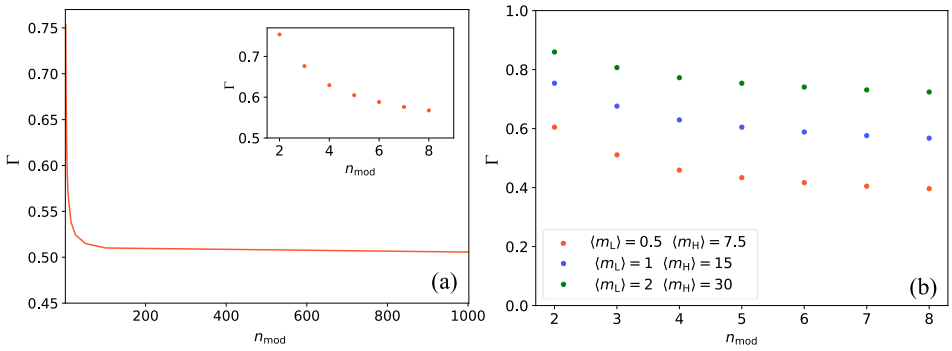


**Fig. 7.** (a) Theoretical expectation of the correlation coefficient Γ as a function of $n_{\mathrm{mod}}$ for $\langle m_{\mathrm{L}} \rangle = 1$ and $\langle m_{\mathrm{H}} \rangle = 15$ and assuming a linear variation of the mean values of the states used to build the amplitude-modulated states. Inset: Enlargement of the behavior for values of $n_{\mathrm{mod}} \leq 8$. (b) The same as in (a) for different energy values of the involved states. Red dots: $\langle m_{\mathrm{L}} \rangle = 0.5$ and $\langle m_{\mathrm{H}} \rangle = 7.5$; blue dots: $\langle m_{\mathrm{L}} \rangle = 1$ and $\langle m_{\mathrm{H}} \rangle = 15$; green dots: $\langle m_{\mathrm{L}} \rangle = 2$ and $\langle m_{\mathrm{H}} \rangle = 30$.

## 5. Conclusions

In this work we have shown the potential of a sum-frequency-based PNR detection system to reveal the amplitude modulation of a light field at telecom wavelengths. In particular, we have studied the statistical features of the modulated states in terms of photon-number distributions and photon-number correlation coefficient. The agreement with the theoretical expectations suggests the implementation of more complex modulation alphabets, such as the APSK states, and the realization of detection schemes involving more than two detectors, such as in the case of the HYNORE receiver, which is quasi optimal in the case of state discrimination problems [56]. The PNR capability of the implemented detection system is also crucial for other kinds of quantum communication protocols, such as for those devoted to QKD [11,57].

**Funding.** Ministero dell'Università e della Ricerca (D.D.M.M. 351/2022, D.D.M.M. 737/2021).

**Acknowledgment.** Scientific support from CRIETT centre of University of Insubria (instrument code: MAC27) is greatly acknowledged. The authors acknowledge Dr. Pietro Anzini (University of Insubria) for the loan of the fiber spectrometer MiniSpectrometer TG-NIR: C11482GA.

**Disclosures.** The authors declare no conflicts of interest.

**Data availability.** Data underlying the results presented in this paper are not publicly available at this time but may be obtained from the authors upon reasonable request.

## References

1. C. H. Bennett, "Quantum cryptography using any two nonorthogonal states," Phys. Rev. Lett. **68**(21), 3121–3124 (1992).
2. B. Huttner, N. Imoto, N. Gisin, *et al.*, "Quantum cryptography with coherent states," Phys. Rev. A **51**(3), 1863–1869 (1995).
3. F. Grosshans and P. Grangier, "Continuous variable quantum cryptography using coherent states," Phys. Rev. Lett. **88**(5), 057902 (2002).
4. N. Gisin, G. Ribordy, W. Tittel, *et al.*, "Quantum cryptography," Rev. Mod. Phys. **74**(1), 145–195 (2002).

Optics EXPRESS


5. G. Cariolaro, *Quantum Communications*, (Springer International Publishing, 2015).
6. J. M. Arrazola and N. Lütkenhaus, "Quantum communication with coherent states and linear optics," Phys. Rev. A **90**(4), 042335 (2014).
7. J. M. Arrazola, M. Karasamanis, and N. Lütkenhaus, "Practical quantum retrieval games," Phys. Rev. A **93**(6), 062311 (2016).
8. M. T. DiMario, L. Kunz, K. Banaszek, *et al.*, "Optimized communication strategies with binary coherent states over phase noise channels," npj Quantum Inf. **5**(1), 65 (2019).
9. Ch. Silberhorn, T. C. Ralph, N. Lütkenhaus, *et al.*, "Continuous variable quantum cryptography: beating the 3 dB loss limit," Phys. Rev. Lett. **89**(16), 167901 (2002).
10. F. Grosshans, G. Van Assche, J. Wenger, *et al.*, "Quantum key distribution using gaussian-modulated coherent states," Nature **421**(6920), 238–241 (2003).
11. M. Cattaneo, M. G. A. Paris, and S. Olivares, "Hybrid quantum key distribution using coherent states and photon-number-resolving detectors," Phys. Rev. A **98**(1), 012333 (2018).
12. A. Leverrier and P. Grangier, "Unconditional security proof of long-distance continuous-variable quantum key distribution with discrete modulation," Phys. Rev. Lett. **102**(18), 180504 (2009).
13. T. Hirano, T. Ichikawa, T. Matsubara, *et al.*, "Implementation of continuous-variable quantum key distribution with discrete modulation," Quantum Sci. Technol. **2**(2), 024010 (2017).
14. S. Ghorai, P. Grangier, E. Diamanti, *et al.*, "Asymptotic security of continuous-variable quantum key distribution with a discrete modulation," Phys. Rev. X **9**(2), 021059 (2019).
15. L. Kunz, M. T. DiMario, F. E. Becerra, *et al.*, "Beating the standard quantum limit for binary constellations in the presence of phase noise," in *21st International Conference on Transparent Optical Networks (ICTON)*, (2019) pp. 1–6.
16. S. Izumi, M. Takeoka, M. Fujiwara, *et al.*, "Displacement receiver for phase-shift-keyed coherent states," Phys. Rev. A **86**(4), 042328 (2012).
17. C. R. Müller and Ch. Marquardt, "A robust quantum receiver for phase shift keyed signals," New J. Phys. **17**(3), 032003 (2015).
18. F. E. Becerra, J. Fan, G. Baumgartner, *et al.*, "Experimental demonstration of a receiver beating the standard quantum limit for multiple nonorthogonal state discrimination," Nat. Photonics **7**(2), 147–152 (2013).
19. F. E. Becerra, J. Fan, and A. Migdall, "Implementation of generalized quantum measurements for unambiguous discrimination of multiple non-orthogonal coherent states," Nat. Commun. **4**(1), 2028 (2013).
20. D. Sych and G. Leuchs, "Coherent state quantum key distribution with multi letter phase-shift keying," New J. Phys. **12**(5), 053019 (2010).
21. C. Häger, A. Graell i Amat, A. Alvarado, *et al.*, "Design of APSK constellations for coherent optical channels with nonlinear phase noise," IEEE Trans. Commun. **68**, 3362–3373 (2013).
22. C. M. Thomas, M. Y. Weidner, and S. H. Durrani, "Digital amplitude-phase keying with M-ary alphabets," IEEE Trans. Commun. **22**(2), 168–180 (1974).
23. E. Biglieri, "High-level modulation and coding for nonlinear satellite channels," IEEE Trans. Commun. **32**(5), 616–626 (1984).
24. R. De Gaudenzi, A. Guillén i Fàbregas, and A. Martinez, "Performance analysis of turbo-coded APSK modulations over nonlinear satellite channels," IEEE Trans. Wireless Commun. **5**(9), 2396–2407 (2006).
25. W. Sung, S. Kang, P. Kim, *et al.*, "Performance analysis of APSK modulation for DVB-S2 transmission over nonlinear channels," Int. J. Commun. Syst. Network **27**(6), 295–311 (2009).
26. M. N. Notarnicola, S. Olivares, E. Forestieri, *et al.*, "Probabilistic amplitude shaping for continuous-variable quantum key distribution with discrete modulation over a wiretap channel," IEEE Trans. Commun. **72**(1), 375–386 (2024).
27. S. Olivares, S. Cialdi, F. Castelli, *et al.*, "Homodyne detection as a near-optimum receiver for phase-shift-keyed binary communication in the presence of phase diffusion," Phys. Rev. A **87**(5), 050303 (2013).
28. E. Diamanti, H.-K. Lo, and B. Qi, "Practical challenges in quantum key distribution," npj Quantum Inf. **2**(1), 16025 (2016).
29. M. Bina, A. Allevi, M. Bondani, *et al.*, "Homodyne-like detection for coherent state-discrimination in the presence of phase noise," Opt. Express **25**(9), 10685–10692 (2017).
30. S. Cassina, M. N. Notarnicola, S. Olivares, *et al.*, "On the application of a Silicon photomultiplier-based receiver for binary phase-shift-keying protocols," Phys. Lett. A **541**, 130403 (2025).
31. A. Sanvito, S. Cassina, M. Lamperti, *et al.*, "Assessing a binary quantum channel exploiting a silicon photomultiplier based hybrid receiver," Opt. Express **32**(22), 39846–39859 (2024).
32. X. Zhang, W.-J. Zhou, H. Zhang, *et al.*, "NbN superconducting nanowire single-photon detector with 90.5% saturated system detection efficiency and 14.7 ps system jitter at 1550 nm wavelength," IEEE J. Sel. Top. Quantum Electron. **28**(5: Lidars and Photonic Radars), 1–8 (2022).
33. E. Schmidt, E. Reutter, M. Schwartz, *et al.*, "Characterization of a photon-number resolving SNSPD using Poissonian and sub-Poissonian light," IEEE Trans. Appl. Supercond. **29**(5), 1–5 (2019).
34. T. Gerrits, N. Thomas-Peter, J. C. Gates, *et al.*, "On-chip, photon-number-resolving, telecommunication-band detectors for scalable photonic information processing," Phys. Rev. A **84**(6), 060301 (2011).
35. J. C. Campbell, "Recent advances in telecommunications avalanche photodiodes," J. Lightwave Technol. **25**(1), 109–121 (2007).

Optics EXPRESS


36. E. Pomarico, B. Sanguinetti, R. Thew, *et al.*, "Room temperature photon number resolving detector for infared wavelengths," Opt. Express **18**(10), 10750–10759 (2010).
37. K. Huang, X. Gu, M. Ren, *et al.*, "Photon-number-resolving detection at 1.04$\mu$m via coincidence frequency upconversion," Opt. Lett. **36**(9), 1722–1724 (2011).
38. K. Huang, Y. Wang, J. Fang, *et al.*, "Mid-infrared photon counting and resolving via efficient frequency upconversion," Photonics Res. **9**(2), 259–265 (2021).
39. S. Cassina, A. Pozzoli, G. Vesco, *et al.*, "Sum-frequency-based photon-number-resolving detector for telecom wavelengths," submitted for publication and quant-ph/2508.02203.
40. J. H. Marburger, "Self-focusing: Theory," Prog. Quantum Electron. **4**, 35–110 (1975).
41. R. W. Boyd, *Nonlinear Optics*, 3rd ed., (Elsevier, 2008).
42. J. L. Debethune, "Quantum correlation functions for radiation fields with stationary independent modes," Il Nuovo Cimento **12**(1), 101–117 (1972).
43. P. Chmela, Z. Ficek, and S. Kielich, "Classical theory of non-degenerate sum-frequency generation by incoherent nonlinear optical mixing of coherent and chaotic radiations," Czech. J. Phys. B **39**(5), 509–528 (1989).
44. A. Allevi, M. Bondani, and A. Andreoni, "Photon-number correlations by photon-number resolving detectors," Opt. Lett. **35**(10), 1707–1709 (2010).
45. P. Diament and M. C. Teich, "Photoelectron-counting distributions for irradiance-modulated radiation," J. Opt. Soc. Am. **60**(5), 682–689 (1970).
46. P. R. Prucnal and M. C. Teich, "Statistical properties of counting distributions for intensity-modulated sources," J. Opt. Soc. Am. **69**(4), 539 (1979).
47. A. Allevi, S. Olivares, and M. Bondani, "Bracket states for communication protocols with coherent states," Int. J. Quantum Inform. **12**(02), 1461018 (2014).
48. G. Chesi, L. Malinverno, A. Allevi, *et al.*, "Measuring nonclassicality with silicon photomultipliers," Opt. Lett. **44**(6), 1371–1374 (2019).
49. G. Chesi, L. Malinverno, A. Allevi, *et al.*, "Optimizing silicon photomultipliers for Quantum optics," Sci. Rep. **9**(1), 7433 (2019).
50. S. Cassina, A. Allevi, V. Mascagna, *et al.*, "Exploiting the wide dynamic range of silicon photomultipliers for quantum optics applications," EPJ Quantum Technol. **8**(1), 4 (2021).
51. J. Lin, Y. Sun, W. Wu, *et al.*, "High-speed photon-number-resolving detection via a GHz-gated SiPM," Opt. Express **30**(5), 7501–7510 (2022).
52. L. Razzoli, A. Pozzoli, and A. Allevi, "Hybrid discrimination strategy in quantum communication based on photon-number-resolving detectors and mesoscopic twin-beam states," Quantum Sci. Technol. **10**(4), 045036 (2025).
53. W. Kang, B. Li, Y. Liang, *et al.*, "Coincidence-pumping upconversion detector based on passively synchronized fiber laser system," IEEE Photonics Technol. Lett. **32**(4), 184–187 (2020).
54. M. Bondani, A. Allevi, and A. Andreoni, "Light statistics by non-calibrated linear photodetectors," Adv. Sci. Lett. **2**(4), 463–468 (2009).
55. A. Allevi, S. Olivares, and M. Bondani, "Manipulating the non-Gaussianity of phase-randomized coherent states," Opt. Express **20**(22), 24850–24855 (2012).
56. M. N. Notarnicola, M. G. A. Paris, and S. Olivares, "Hybrid near-optimum binary receiver with realistic photon-number-resolving detectors," J. Opt. Soc. Am. B **40**(4), 705 (2023).
57. M. N. Notarnicola, M. Jarzyna, S. Olivares, *et al.*, "Optimizing state-discrimination receivers for continuous-variable quantum key distribution over a wiretap channel," New J. Phys. **25**(10), 103014 (2023).